J|A|C|S ARTICLES

Published on Web 05/07/2009

Halogen Photoreductive Elimination from Gold(III) Centers

Thomas S. Teets and Daniel G. Nocera*

Department of Chemistry, 6-335, Massachusetts Institute of Technology, 77 Massachusetts Avenue, Cambridge, Massachusetts 02139-4307

Received February 10, 2009; E-mail: nocera@mit.edu

Abstract: Monomeric complexes of the type $Au^{III}(PR_3)X_3$ and bimetallic complexes of the type $Au_2^{I,III}[\mu\text{-}CH_2(R_2P)_2]X_4$ and $Au_2^{III,III}[\mu\text{-}CH_2(R_2P)_2]X_6$ (R = Ph, Cy, X = Cl^-, Br^-) undergo facile photoelimination of halogen. M−X bond activation and halogen elimination is achieved upon LMCT excitation of solutions of Au^{III} complexes in the presence of olefin chemical traps. As opposed to the typical one-electron redox transformations of LMCT photochemistry, the LMCT photochemistry of the Au^{III} centers allows for the unprecedented (i) two-electron photoelimination of X_2 from a monomeric center and (ii) four-electron photoelimination of X_2 from a bimetalllic center. The quantum yields for X_2 photoproduction, in general, are between 10% and 20% for all species, showing only minimal dependence on the identity of the ligands about gold, or the nuclearity of the complex. Efficient X_2 photoelimination is observed in the absence of a chemical trap, providing a rare example of authentic, trap-free halogen elimination from a transition metal center.

Introduction

Solar energy will not be used as a large-scale energy supply for society unless it can be stored.[1,2] The highest energy density for the storage of solar energy is in chemical bonds, thus defining an imperative for developing catalysts that promote fuel-forming reactions. A pre-eminent energy-storing reaction is water-splitting,[3,4] though the transformation of this small molecule presents formidable challenges. This water-to-hydrogen fuel conversion is accompanied by the removal of four protons and four electrons from water to produce oxygen.[5,6] Hydrogen can be produced in simpler two-electron, two-proton reactions[7] of which HX (X = Cl or Br) splitting possesses nearly equivalent energy storage to that of H_2O splitting. The efficiency of HX splitting is typically not limited by the reductive H_2 half-reaction but rather by the oxidative X_2 half-reaction. Hence, the success of HX energy storage depends crucially on using light to drive the unfavorable energetics associated with X_2 production. Most examples of X_2 photoelimination occur from organic substrates and by using high-energy light.[8−11] The photoelimination of halogen from metal centers is rare and typically driven by the presence of a trap;[12−14] only with a trap can appreciable quantities of H_2 be photoproduced from HX.[15,16] An obvious strategy for improving the H_2 production from HX is to increase the quantum yield of M−X bond activation and ultimately effect X_2 photoproduction without the need for trap so that maximal energy may be stored.

The quantum efficiency of X_2 elimination may be enhanced by using late transition metal complexes in high oxidation states to drive M−X photoactivation. Whereas the $Rh^{II}-Au^{II}$ complex, $[Rh^{II}Au^{II}(tfepma)_2(CN^tBu)_2Cl_3]AuCl_2$ (tfepma = $CH_3N(P[OCH_2CF_3]_2)_2$), is thermally unstable, a stable d^7-d^9 complex may be realized by replacing Rh(II) with Pt(III). The $[Pt^{III}Au^{II}(dppm)_2PhCl_3]PF_6$ (dppm = bis(diphenylphosphino)methane) complex is photoreduced to its $Pt^{II}Au^{I}$ congener upon irradiation in the presence of 2,3-dimethyl-1,3-butadiene. The quantum yield of halogen elimination achieves a maximum of 5.7% at 5 M trap concentration, nearly a 10-fold increase over halogen elimination from a d^7-d^9 $Rh^{II}-Rh^0$ bimetallic core.[17,18] Even higher quantum yields are obtained from more highly oxidizing $Pt^{III}-Pt^{III}$ cores. $Pt_2^{III,III}(tfepma)_2Cl_6$ undergoes efficient two-electron photoreduction (Φ = 38%) at high trap concentrations and is able to eliminate Cl_2 when irradiated in the solid state,

(1) Lewis, N. S.; Nocera, D. G. *Proc. Natl. Acad. Sci. U.S.A.* **2006**, *103*, 15729–15735.
(2) Kanan, M. W.; Surendranath, Y.; Nocera, D. G. *Chem. Soc. Rev.* **2009**, *38*, 109–114.
(3) Kanan, M. W.; Nocera, D. G. *Science* **2008**, *321*, 1072–1075.
(4) Surendranath, Y.; Dinèa, M.; Nocera, D. G. *J. Am. Chem. Soc.* **2009**, *131*, 2615–2620.
(5) Eisenberg, R.; Gray, H. B. *Inorg. Chem.* **2008**, *47*, 1697–1699.
(6) Betley, T. A.; Wu, Q.; Van Voorhis, T.; Nocera, D. G. *Inorg. Chem.* **2008**, *47*, 1849–1861.
(7) Esswein, A. J.; Nocera, D. G. *Chem. Rev.* **2007**, *107*, 4022–4047.
(8) Miranda, M. A.; Pérez-Prieto, J.; Font-Sanchis, E.; Scaiano, J. C. *Acc. Chem. Res.* **2001**, *34*, 717–726.
(9) Marvet, U.; Brown, E. J.; Dantus, M. *Phys. Chem. Chem. Phys.* **2000**, *2*, 885–891.
(10) Rozgonyi, T.; González, L. *J. Phys. Chem. A* **2002**, *106*, 11150–11161.
(11) Görner, H. *J. Photochem. Photobiol. A* **1995**, *90*, 57–63.
(12) Esswein, A. J.; Dempsey, J. L.; Nocera, D. G. *Inorg. Chem.* **2007**, *46*, 2362–2364.
(13) Cook, T. R.; Esswein, A. J.; Nocera, D. G. *J. Am. Chem. Soc.* **2007**, *129*, 10094–10095.
(14) Esswein, A. J.; Veige, A. S.; Nocera, D. G. *J. Am. Chem. Soc.* **2005**, *127*, 16641–16651.
(15) Heyduk, A. F.; Nocera, D. G. *Science* **2001**, *293*, 1639–1641.
(16) Esswein, A. J.; Veige, A. S.; Nocera, D. G. *J. Am. Chem. Soc.* **2005**, 127–16641.
(17) Heyduk, A. F.; Macintosh, A. M.; Nocera, D. G. *J. Am. Chem. Soc.* **1999**, *121*, 5023–5032.
(18) Odom, A. L.; Heyduk, A. F.; Nocera, D. G. *Inorg. Chim. Acta* **2000**, *297*, 330–337.

providing what is the first example of authentic, trap-free X_2 reductive photoelimination from a transition-metal center.[19]

We now generalize X_2 photoelimination by showing that the reaction may proceed efficiently from Au^{III} centers of mono- and bimetallic cores without the need for a halogen trap. Despite thorough characterization of the photophysical properties of Au^I compounds,[20−25] photochemical transformations involving molecular gold compounds are limited, particularly for Au^{III}.[26,27] Reductive elimination from Au^{III} centers involves carbon−carbon bond formations,[28−30] frequently from Au^{III} species of the type $LAuR_2X$ (L = phosphine, R = alkyl or aryl, X = halide). Though the light-sensitivity of some Au_2^{II} and Au^{III} halide species has been noted,[31] a well-defined halogen elimination photochemistry from gold has eluded characterization.[32] The two-electron $Au^{III/I}$ redox couple is well matched to the two-electron equivalency of halogen photoreductive elimination. Hence, we were attracted to the possibility of effecting two- and four-electron halogen photoelimination reactions from mono- and bimetallic complexes, respectively. The suite of Au^{III} compounds listed in Chart 1 permit X_2 photoreductive elimination to be examined for systematically altered metal cores and ligand sets. We make the unique observation that M−X bond activation and authentic X_2 elimination can be achieved by LMCT excitation of complexes lacking a metal−metal bond. Though LMCT photochemistry is conventionally confined to one-electron redox transformations,[33] the LMCT excitation of the Au^{III} centers of Chart 1 allows for (i) the facile four-electron reduction of $Au_2^{III,III}$ complexes to give the corresponding $Au_2^{I,I}$ species and (ii) the unprecedented photoelimination of X_2 from a monomeric metal center. This photochemistry is paralleled by a thermal reaction chemistry on a time scale amenable to kinetic interrogation. Bimetallic $Au_2^{III,III}$ species are observed to reductively eliminate much more rapidly than their Au^{III} monomeric counterparts. Characterization of the haloalkane product resulting from thermal and photochemical reactions in the presence of alkene indicates that the thermal and photochemical reactions proceed by disparate mechanisms. Whereas photoreductive elimination from complexes in solution requires the use of halogen traps, the reaction proceeds smoothly in the solid state in the absence of trap. The X_2 back reaction is prevented by virtue of the production of a volatile X_2 photoproduct. Because X_2 reacts with any of the Au^I centers in Chart 1 to produce the corresponding Au^{III} analogue, the solid state photoinduced elimination of halogen is an energy-storing photoreaction.

Chart 1

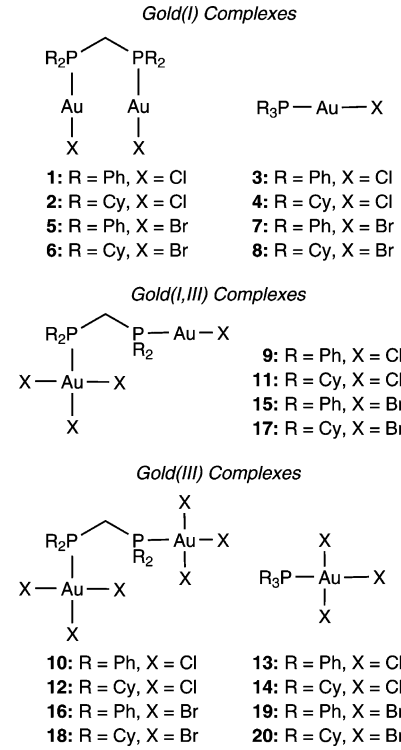

Experimental Section

General Considerations. All solvents were obtained commercially and used as received except for CH_2Cl_2 and THF, which were dried by passage through an alumina column. Air-sensitive phosphines were handled in a nitrogen-filled glovebox. All gold compounds reported here are air-stable and were routinely handled in an ambient atmosphere. The phosphines PPh_3, PCy_3, dppm, and dcpm were obtained from Strem Chemicals, bromine was obtained from Sigma-Aldrich (reagent grade), and chlorine was delivered as the iodobenzene adduct, $PhICl_2$.[34] The starting materials $Au_2^{I,I}(dppm)Cl_2$ (**1**),[35] $Au_2^{I,I}(dcpm)Cl_2$ (**2**),[36] $Au^I(PPh_3)Cl$ (**3**),[22] and $Au^I(PCy_3)Cl$ (**4**)[37] were prepared by reacting stoichiometric amounts of the appropriate phosphine with chloro(tetrahydrothiophene)-gold(I) $[Au^I(tht)Cl]$[38] in THF, followed by precipitation with pentane and isolation by vacuum filtration. Halide exchange to prepare $Au_2^{I,I}(dppm)Br_2$ (**5**), $Au_2^{I,I}(dcpm)Br_2$ (**6**), $Au^I(PPh_3)Br$ (**7**), and $Au^I(PCy_3)Br$ (**8**) was carried out by reaction with excess aqueous KBr, and $Au_2^{I,III}(dppm)Br_4$ (**15**) and $Au^{III}(PPh_3)Br_3$ (**19**) were prepared following known methods.[39] All thermal reductions of Au^{III} were carried out at room temperature in 1 M olefin

(19) Cook, T. R.; Surendranath, Y.; Nocera, D. G. *J. Am. Chem. Soc.* **2009**, *131*, 28–29.
(20) Partyka, D. V.; Esswein, A. J.; Zeller, M.; Hunter, A. D.; Gray, T. G. *Organometallics* **2007**, *26*, 3279–3282.
(21) Teets, T. S.; Partyka, D. V.; Esswein, A. J.; Updegraff, J. B., III; Zeller, M.; Hunter, A. D.; Gray, T. G. *Inorg. Chem.* **2007**, *46*, 6218–6220.
(22) Sinha, P.; Wilson, A. K.; Omary, M. A. *J. Am. Chem. Soc.* **2005**, *127*, 12488–12489.
(23) Forward, J. M.; Bohmann, D.; Fackler, J. P., Jr.; Staples, R. J. *Inorg. Chem.* **1995**, *34*, 6330–6336.
(24) Fernández, E. J.; Laguna, A.; López-de-Luzuriaga, J. M.; Monge, M.; Montiel, M.; Olmos, M. E.; Rodríguez-Castillo, M. *Dalton Trans.* **2006**, 3672–3677.
(25) Yam, V. W.-W.; Cheng, E. C.-C. *Top. Curr. Chem.* **2007**, *281*, 269–309.
(26) Bachman, R. E.; Bodolosky-Bettis, S. A.; Pyle, C. J.; Gray, M. A. *J. Am. Chem. Soc.* **2008**, *130*, 14303–14310.
(27) Serafimova, I. M.; Hoggard, P. E. *Inorg. Chim. Acta* **2002**, *338*, 105–110.
(28) Bennett, M. A.; Bhargava, S. K.; Hockless, D. C. R.; Welling, L. L.; Willis, A. C. *J. Am. Chem. Soc.* **1996**, *118*, 10469–10478.
(29) Komiya, S.; Kochi, J. K. *J. Am. Chem. Soc.* **1976**, *98*, 7599–7607.
(30) Komine, N.; Ichikawa, K.; Mori, A.; Hirano, M.; Komiya, S. *Chem. Lett.* **2005**, *34*, 1704–1705.
(31) Fackler, J. P., Jr. *Inorg. Chem.* **2002**, *41*, 6959–6972.
(32) Vogler, A.; Kunkely, H. *Coord. Chem. Rev.* **2001**, *219−221*, 489–507.
(33) Ronco, S.; Ferraudi, G. Excited State Redox Reactions of Transition Metal Complexes. In *Handbook of Photochemistry and Photobiology*; Nalwa, H. S., Ed.; American Scientific Publishers: Stevenson Ranch, CA, 2003; pp 283−343.
(34) Zielinska, A.; Skulski, L. *Tetrahedron Lett.* **2004**, *45*, 1087–1089.
(35) Schmidbaur, H.; Wohlleben, A.; Wagner, F.; Orama, O.; Huttner, G. *Chem. Ber.* **1977**, *110*, 1748–1754.
(36) Yam, V. W.-W.; Cheung, K.-L.; Yip, S.-K.; Cheung, K.-K. *J. Organomet. Chem.* **2003**, *681*, 196–209.
(37) Isab, A. A.; Fettouhi, M.; Ahmad, S.; Ouahab, L. *Polyhedron* **2003**, *22*, 1349–1354.
(38) Usón, R.; Laguna, A.; Laguna, M. *Inorg. Synth.* **1989**, *26*, 85–91.
(39) Schneider, D.; Schier, A.; Schmidbaur, H. *Dalton Trans.* **2004**, 1995–2005.

solutions; light was rigorously excluded by thoroughly wrapping all reaction vessels in aluminum foil.

Physical Methods. All NMR spectra were recorded at the MIT Department of Chemistry Instrumentation Facility on a Varian Mercury 300 NMR spectrometer or a Varian Inova-500 NMR spectrometer. $^{31}P\{^1H\}$ NMR spectra were referenced to an external standard of 85% D_3PO_4 and ^1H spectra were referenced to TMS using the residual proteo solvent resonances. $^{31}P\{^1H\}$ NMR kinetics experiments were performed at 20 °C using triphenylphosphate as an internal integration standard. $^{31}P\{^1H\}$ spectra of solid-state photolysis samples were quantified with a known concentration of triphenylphosphate as an internal standard; a spectrometer delay time of 30 s was employed. UV−vis spectra were recorded at room temperature in quartz cuvettes on a Varian Cary 5000 UV−vis−NIR spectrophotometer. Extinction coefficients were determined over a concentration range of ∼5−100 μM, for which all compounds obeyed Beer's Law.

Photochemical reactions were performed using a 1000 W high-pressure Hg/Xe arc lamp (Oriel). The beam was passed through a water-jacketed filter holder containing appropriate long pass filters, an iris, and collimating lens. Dichloromethane solutions of samples prepared for large-scale photolysis experiments were contained in standard borosilicate NMR tubes or glass Schlenk tubes. Solid-state photolysis experiments were conducted in a custom-built H-shaped cell with the two compartments separated by a Teflon valve; one of the two compartments was equipped with an inlet and outlet port for gas measurements. To obtain a uniform coating of solid for photolyses experiments, a 10−15 mg sample was dissolved in a minimum amount of CH_2Cl_2, which was deposited in the cell and evaporated under reduced pressure. The entire apparatus was evacuated to <200 mTorr prior to photolysis. The photolysis cell was periodically rotated during irradiation to ensure maximum exposure to the beam. The surface of the sample photolyzed rapidly, though in many cases starting material was observed in the product mixture after >3 h irradiation times. Longer photolysis times did lead to further conversion, at the expense of an increased buildup of side products in the sample. Evolved Cl_2 was collected by opening the valve dividing the two cell compartments and immersing the sample-free compartment in liquid nitrogen. Chlorine was analyzed by mass spectrometric analysis using an Agilent Technologies 5975C mass selective detector operating in electron impact ionization mode. The liquid nitrogen cooled side of the sample cell that contained evolved gases was purged with He carrier gas for two hours until a stable baseline was obtained. The frozen compartment was rapidly warmed by immersion in water and the evolved gases were fed into the mass spectrometer for real-time analysis. Data were collected until all gas levels returned to near baseline values. The mass spectrometer was operated in selective ion mode that monitored for 35 (Cl_2 fragment), 37 (Cl_2 fragment), 70 (Cl_2), 72 (Cl_2), and 74 (Cl_2) amu ions. The three Cl_2 ions gave very weak signals and were not considered in the data analysis. Evolved Br_2 was collected in a similar fashion to the methods employed for Cl_2, except that the frozen cell compartment was precharged with 5 mL of distilled water. The resulting aqueous Br_2 solution was analyzed by DPD titrimetry.[40]

For solution quantum yield experiments, samples were contained in a quartz cuvette equipped with a Teflon-coated magnetic stir bar. Monochromatic light was generated by combining the output from a long-pass filter with a Hg line filter of 320 nm for Au^{III} chlorides and 370 nm for Au^{III} bromides. Potassium ferrioxalate was synthesized via a published procedure and used as a chemical actinometer.[41] The photon flux was determined from the average of the actinometric measurements collected before and after irradiation of a set of three samples. UV−vis spectra for quantum yield measurements were recorded on a Spectral Instruments 400 diode array spectrophotometer and were blanked to the appropriate solvent.

Preparation of $Au_2^{I,III}(dppm)Cl_4$ (9). To a solution of **1** (100 mg, 0.118 mmol) in 5 mL of CH_2Cl_2, was added dropwise a solution of $PhICl_2$ (34 mg, 0.12 mmol, 1.0 equiv) in 1 mL of CH_2Cl_2. The resulting solution was stirred for 12 h in the dark during which some product precipitated. The mixture was layered with ∼15 mL of pentane and stored at −20 °C for 1 day. **9** formed as a microcrystalline pale yellow solid. The supernatant was decanted, and the remaining solid product washed with 2 × 15 mL pentane and dried in vacuo. Yield: 100 mg (92.3%). ^1H NMR (500 MHz, CD_2Cl_2): δ 7.81−7.87 (m, 4H), 7.56−7.62 (m, 2H), 7.47−7.55 (m, 6H), 7.36−7.46 (m, 8H) 4.27 (dd, J_{H-P} = 11 Hz, 13 Hz, 2H). $^{31}P\{^1H\}$ NMR (121.5 MHz, CD_2Cl_2): δ 36.2 (d, J_{P-P} = 17 Hz), 18.5 (d, J_{P-P} = 16 Hz). UV−vis (CH_2Cl_2): λ/nm {ε/(M^{-1} cm^{-1})} 341 {9400}. Anal. Calcd for $C_{25}H_{22}Au_2Cl_4P_2$: C, 32.63; H, 2.41. Found: C, 32.82; H, 2.51.

Preparation of $Au_2^{III,III}(dppm)Cl_6$ (10). A sample of $PhICl_2$ (68 mg, 0.25 mmol, 2.1 equiv) in 2 mL of CH_2Cl_2 was added to a stirred solution of **1** (100 mg, 0.118 mmol) in 8 mL of CH_2Cl_2. The yellow solution was stirred in the dark for 17 h and then was concentrated to ∼4 mL, at which time a yellow solid began to precipitate. Addition of 15 mL of pentane gave the product as a yellow solid, which was separated from the supernatant by decantation, washed with 2 × 15 mL pentane and dried in vacuo. Yield: 101 mg of **10**·0.5CH_2Cl_2 (83.0%). ^1H NMR (500 MHz, $CDCl_3$): δ 7.75−7.82 (m, 12H), 7.61−7.66 (m, 8H), 5.12 (t, J_{H-P} = 15 Hz, 2H). $^{31}P\{^1H\}$ NMR (121.5 MHz, $CDCl_3$): δ 29.2 (s). UV−vis (CH_2Cl_2): λ/nm {ε/(M^{-1} cm^{-1})} 339 {16000}. Anal. Calcd for $C_{25}H_{22}Au_2Cl_6P_2$·0.5CH_2Cl_2: C, 29.63; H, 2.24. Found: C, 29.43; H, 2.37.

Preparation of $Au_2^{I,III}(dcpm)Cl_4$ (11). A sample of **2** (100 mg, 0.114 mmol) was dissolved in 10 mL of CH_2Cl_2. A solution of $PhICl_2$ (32 mg, 0.12 mmol, 1.1 equiv) in 1 mL of CH_2Cl_2 was added dropwise to give a yellow solution, which was stirred at room temperature for 3 h. The volatiles were removed to give a yellow residue, which was redissolved in 2 mL of CH_2Cl_2 and slowly added to 15 mL of pentane to furnish a yellow solid. The supernatant was decanted and the resulting solid material was washed with pentane and dried in vacuo. Yield: 93 mg (86%). ^1H NMR (500 MHz, $CDCl_3$): δ 3.39−3.51 (br, m, 2H), 2.93 (dd, J_{H-P} = 11 Hz, 14 Hz, 2H), 2.30−2.41 (br, m, 2H), 1.68−2.24 (br, m, 24H), 1.19−1.62 (br, m, 16H). $^{31}P\{^1H\}$ NMR (121.5 MHz, $CDCl_3$): δ 60.0 (d, J_{P-P} = 9 Hz), 35.9 (d, J_{P-P} = 9 Hz). UV−vis (CH_2Cl_2): λ/nm {ε/(M^{-1} cm^{-1})} 327 {8500}. Anal. Calcd for $C_{25}H_{46}Au_2Cl_4P_2$: C, 31.80; H, 4.91. Found: C, 32.31; H, 4.96.

Preparation of $Au_2^{III,III}(dcpm)Cl_6$ (12). A solution of $PhICl_2$ (66 mg, 0.24 mmol, 2.1 equiv) in 1.5 mL of CH_2Cl_2 was added to **2** (100 mg, 0.114 mmol) in 10 mL of CH_2Cl_2. The yellow solution was stirred in the dark for 16 h, at which time the volatiles were removed via rotary evaporation to leave a yellow residue. The residue was taken up in ∼2 mL of CH_2Cl_2 and added dropwise to 15 mL of pentane, prompting a pale yellow solid to separate. The supernatant was decanted and the solid was washed with pentane and dried in vacuo. Yield: 98 mg (84%). ^1H NMR (500 MHz, $CDCl_3$): δ 3.64 (t, J_{H-P} = 14 Hz, 2H), 3.14−3.24 (br, m, 4H), 2.19−2.31 (br, m, 8H), 1.79−2.02 (br, m, 20H), 1.33−1.50 (br, m, 12H). $^{31}P\{^1H\}$ NMR (121.5 MHz, $CDCl_3$): δ 60.3 (s). UV−vis (CH_2Cl_2): λ/nm {ε/(M^{-1} cm^{-1})} 328 {16 000}. Anal. Calcd for $C_{25}H_{46}Au_2Cl_6P_2$: C, 29.58; H, 4.57. Found: C, 29.96; H, 4.60.

(40) Eaton, A. D.; Clesceri, L. S.; Rice, W. E.; Greenberg, A. E. *Standard Methods for the Examination of Water and Wastewater*, 21st ed.; American Public Health Association, American Water Works Association, Water Pollution Control Federation: Washington, DC, 2005; Chapter 4.

(41) Montalti, M.; Credi, A.; Prodi, L.; Gandolfi, M. T. *Handbook of Photochemistry*, 3rd ed.; Taylor and Francis: Boca Raton, FL, 2006.

Preparation of $Au^{III}(PPh_3)Cl_3$ (13). This compound has been reported previously by oxidation with Cl_2 gas.[27,42] Here we report the preparation using $PhICl_2$. To a solution of **3** (100 mg, 0.202 mmol) in 2 mL of CH_2Cl_2 was added a solution of $PhICl_2$ (58 mg, 0.21 mmol, 1.0 equiv) in 2 mL of CH_2Cl_2. After stirring for 8 h at room temperature in the dark, the solution was concentrated to <1 mL, and ~15 mL of pentane was added to afford the product as a yellow powder. The solvent mixture was decanted and the solid was washed with pentane dried in vacuo. Yield: 95 mg (83%). ^{1}H NMR (500 MHz, $CDCl_3$): δ 7.66−7.75 (m, 9H), 7.54−7.60 (m, 6H). $^{31}P\{^1H\}$ NMR (121.5 MHz, $CDCl_3$): δ 44.3 (s). UV−vis (CH_2Cl_2): λ/nm {ε/(M^{-1} cm^{-1})} 336 {13 000}. Anal. Calcd for $C_{18}H_{15}AuCl_3P$: C, 38.22; H, 2.67. Found: C, 38.23; H, 2.66.

Preparation of $Au^{III}(PCy_3)Cl_3$ (14). A sample of **4** (100 mg, 0.195 mmol) was dissolved in 1.5 mL of CH_2Cl_2. To this solution was added $PhICl_2$ (56 mg, 0.20 mmol, 1.03 equiv) in 1.5 mL of CH_2Cl_2. The resulting yellow solution was stirred in the dark at room temperature for 8 h. After concentrating to <1 mL, 15 mL of pentane was added to separate **14** as a pale yellow solid. The supernatant was decanted and the product was washed with pentane and dried in vacuo. Yield: 100 mg (87.8%). ^{1}H NMR (500 MHz, $CDCl_3$): δ 2.95−3.06 (br, m, 3H), 2.00−2.08 (br, m, 6H), 1.86−1.96 (br, m, 6H), 1.68−1.84 (br, m, 9H) 1.27−1.40 (br, m, 9H). $^{31}P\{^1H\}$ NMR (121.5 MHz, $CDCl_3$): δ 74.8 (s). UV−vis (CH_2Cl_2): λ/nm {ε/(M^{-1} cm^{-1})} 253 {12 000}, 328 {8700}. Anal. Calcd for $C_{18}H_{33}AuCl_3P$: C, 37.03; H, 5.70. Found: C, 37.25; H, 5.63.

Preparation of $Au_2^{III,III}(dppm)Br_6$ (16). To a solution of **5** (86 mg, 0.091 mmol) in 4 mL of CH_2Cl_2 was added a solution of Br_2 (36 mg, 0.228 mmol, 2.5 equiv) in 2 mL of CH_2Cl_2. The solution turned red immediately and was stirred in the dark for 90 min. The reaction mixture was layered with pentane and stored at −20 °C to give red crystals of **16**. The supernatant was decanted and the product was washed with pentane and dried in vacuo. Yield: 111 mg (96.3%). ^{1}H NMR (500 MHz, $CDCl_3$): δ 7.69−7.80 (m, 12H), 7.57−7.62 (m, 8H), 5.42 (t, J_{H-P} = 14 Hz, 2H). $^{31}P\{^1H\}$ NMR (121.5 MHz, $CDCl_3$): δ 14.6 (s). UV−vis (CH_2Cl_2): λ/nm {ε/(M^{-1} cm^{-1})} 256 {56 000}, 349 {12 000}. Anal. Calcd for $C_{25}H_{22}Au_2Br_6P_2$: C, 23.87; H, 1.76. Found: C, 24.12; H, 2.04.

Preparation of $Au_2^{I,III}(dcpm)Br_4$ (17). To a solution of **6** (100 mg, 0.104 mmol) in 6 mL of CH_2Cl_2 was added dropwise a solution of Br_2 (17 mg, 0.11 mmol, 1.05 equiv) in 1 mL of CH_2Cl_2. The solution turned red immediately and was stirred at room temperature for 3.5 h in exlusion of light. The solution was concentrated to ~2 mL, and addition of 15 mL pentane gave the product as a salmon-colored powder. The solvents were decanted and the material was washed with pentane and dried in vacuo. Yield: 98 mg (84%). ^{1}H NMR (500 MHz, $CDCl_3$): δ 3.63−3.73 (br, m, 2H), 2.92 (dd, J_{H-P} = 10 Hz, 14 Hz, 2H), 2.40−2.50 (br, m, 2H), 2.21−2.30 (br, m, 2H), 1.20 − 2.19 (br, m, 38H). $^{31}P\{^1H\}$ NMR (121.5 MHz, $CDCl_3$): δ 45.0 (s), 37.6 (s). UV−vis (CH_2Cl_2): λ/nm {ε/(M^{-1} cm^{-1})} 253 {19 000}, 397 {3900}. Anal. Calcd for $C_{25}H_{46}Au_2Br_4P_2$: C, 26.76; H, 4.13. Found: C, 27.12; H, 4.12.

Preparation of $Au_2^{III,III}(dcpm)Br_6$ (18). A sample of **6** (100 mg, 0.104 mmol) was dissolved in 6 mL of CH_2Cl_2. A solution of Br_2 (62 mg, 0.38 mmol, 3.7 equiv) in 1 mL of CH_2Cl_2 was added. The resulting red solution was stirred in exclusion of light for 6 h. After concentrating to ~1 mL, 15 mL of pentane was added to give a dark red solid, which was separated by decantation, washed with 2 × 15 mL pentane and dried in vacuo. Yield: 116 mg (87.1%). ^{1}H NMR (500 MHz, $CDCl_3$): δ 3.89 (t, J_{H-P} = 14 Hz, 2H), 3.24−3.34 (br, m, 4H), 2.23−2.31 (br, m, 8H), 1.76−2.00 (br, m, 20H), 1.35−1.50 (br, m, 12H). $^{31}P\{^1H\}$ NMR (121.5 MHz, $CDCl_3$): δ 48.4 (s). UV−vis (CH_2Cl_2): λ/nm {ε/(M^{-1} cm^{-1})} 254 {33 000}, 401 {7300}. Anal. Calcd for $C_{25}H_{46}Au_2Br_6P_2$: C, 23.42; H, 3.62. Found: C, 23.42; H, 3.56.

Preparation of $Au^{III}(PCy_3)Br_3$ (20). To a solution of **8** (100 mg, 0.179 mmol) in 1.5 mL of CH_2Cl_2 was added a solution of Br_2 (62 mg, 0.39 mmol, 2.2 equiv) in 1 mL of CH_2Cl_2. The dark red solution was shielded from light and stirred for 2 h, at which time it was concentrated to ~1 mL. Addition of 15 mL of pentane gave an orange solid, which was washed with pentane and dried in vacuo. Yield: 116 mg (90.4%). ^{1}H NMR (500 MHz, $CDCl_3$): δ 3.08−3.21 (br, m, 3H), 2.01−2.12 (br, m, 6H), 1.65−1.95 (br, m, 15H), 1.29−1.42 (br, m, 9H). $^{31}P\{^1H\}$ NMR (121.5 MHz, $CDCl_3$): δ 65.0 (s). UV−vis (CH_2Cl_2): λ/nm {ε/(M^{-1} cm^{-1})} 250 {23 000}, 279 {18 000}, 400 {5700}. Anal. Calcd for $C_{18}H_{33}AuBr_3P$: C, 30.15; H, 4.64. Found: C, 30.16; H, 4.65.

X-ray Crystallographic Details. Single crystals of **2** were obtained from a 1,1,2,2-tetrachloroethane solution layered with heptane, **9**, **10**, **14**, **16**, and **20** were crystallized from CH_2Cl_2 solutions layered with pentane, crystals of **17** were grown from a chlorobenzene solution layered with heptane, and crystals of **18** were obtained from a 1,2-dichloroethane solution layered with heptane. The crystals were mounted on a Bruker three circle goniometer platform equipped with an APEX detector. A graphic monochromator was employed for wavelength selection of the Mo Kα radiation (μ = 0.71073 Å). The data were processed and refined using the program SAINT supplied by Siemens Industrial Automation. Structures were solved by direct methods in SHELXS and refined by standard difference Fourier techniques in the SHELXTL program suite (v. 6.10, Sheldrick G. M., and Siemens Industrial Automation, 2000). Hydrogen atoms were placed in calculated positions using the standard riding model and refined isotropically; all other atoms were refined anisotropically. A positional disorder of the three bromine atoms bonded to Au(2) in the structure of **16** was modeled. In the same structure, the CH_2Cl_2 solvate was modeled as a two-part disorder. In the structure of **18**, one of the two independent dichloroethane solvates was modeled as a two-part disorder. In the structure of **2**, the C−C distances of the solvent molecule were restrained to a reasonable value (1.54 Å) using a DFIX command. The 1−2 and 1−3 distances of all disordered parts were restrained to be similar using the SADI command; the rigid-bond restraints SIMU and DELU were also used on disordered parts. Unit cell parameters, morphology, and solution statistics for the structures of **2**, **9**, **10**, **14**, **16**, **17, 18**, and **20** are summarized in Table 1. All thermal ellipsoid plots are drawn at 50% probability level, with hydrogen atoms and solvent molecules omitted.

Results

Synthesis and Characterization. Monomeric and dimeric Au^I chloride precursors were synthesized by stoichiometric reaction of the appropriate phosphine with the versatile Au^I starting material $Au^I(tht)Cl$.[38] Conversion of chloride complexes **1**−**4** to the bromide complexes **5**−**8** was accomplished by reacting a CH_2Cl_2 solution of the chloride precursor with a 5-fold excess of aqueous KBr. This metathesis method has proven to be general for halide exchange of phosphine-ligated Au^I species.[39] In a slight variation of precedent, oxidation of **1**−**4** to prepare dimeric $Au_2^{I,III}$ or $Au_2^{III,III}$ (**9**−**12**) and monomeric Au^{III} complexes (**13**, **14**) was performed in CH_2Cl_2 using $PhICl_2$ to deliver chlorine. Though the reactions are slower than direct Cl_2 oxidation, in some cases requiring 12+ h to complete, the stoichiometry is very easy to control using solid $PhICl_2$ as the source of chlorine. All reactions proceeded cleanly and quantitatively as judged by ^{31}P NMR spectra of reaction mixtures. Oxidation of **5**−**8** with Br_2 in CH_2Cl_2 gave gold(III)-containing **15**−**20**; complexes **15** and **19** have been previously reported by the same procedure. All Au^{III} complexes were obtained in isolated yields of >80% and gave satisfactory microanalyses.

Oxidation of dimeric $Au_2^{I,I}$ species with a single equivalent of halogen can potentially produce either $Au_2^{II,II}$ or $Au_2^{I,III}$ complexes. For the bimetallic compounds reported here, room

(42) Attar, S.; Nelson, J. H.; Bearden, W. H.; Alcock, N. W.; Solujiæ, L.; Milosacljeviæ, E. B. *Polyhedron* **1991**, *10*, 1939–1949.

Table 1. Crystallographic Summary for Complexes **2**, **9**, **10**, **12**, **14**, **16**, **17**, **18**, and **20**

	2·2.5$C_2H_2Cl_4$	**9**	**10**·CH_2Cl_2	**14**	**16**·CH_2Cl_2	**17**	**18**·$C_2H_4Cl_2$	**20**
formula	$C_{30}H_{51}Au_2Cl_{12}P_2$	$C_{25}H_{22}Au_2Cl_4P_2$	$C_{26}H_{24}Au_2Cl_8P_2$	$C_{18}H_{33}AuCl_3P$	$C_{26}H_{24}Au_2Br_6Cl_2P_2$	$C_{25}H_{46}Au_2Br_4P_2$	$C_{27}H_{50}Au_2Br_6Cl_2P_2$	$C_{18}H_{33}AuBr_3P$
fw, g/mol	1292.98	920.1	1075.83	583.73	1342.69	1122.13	1380.90	717.11
temperature, K	100(2)	100(2)	100(2)	100(2)	100(2)	100(2)	100(2)	100(2)
cryst syst	trigonal	orthorhombic	monoclinic	monoclinic	triclinic	monoclinic	monoclinic	orthorhombic
space group	$P3_221$	$P2_12_12_1$	$P2_1/n$	$C2/c$	$P\bar{1}$	$P2_1/n$	$P2_1/n$	$Pnma$
color	colorless	yellow	yellow	yellow	red	red	red	orange
a (Å)	15.787(2)	12.570(3)	9.9293(6)	17.2194(14)	11.2927(12)	11.7519(9)	9.5914(8)	14.7919(9)
b (Å)	15.787(2)	13.011(3)	14.9256(9)	13.7859(14)	12.2466(13)	14.3982(10)	15.0383(13)	16.4575(10)
c (Å)	30.811(4)	16.508(3)	21.1774(13)	18.2238(16)	15.2241(15)	19.2592(14)	26.602(2)	9.0123(5)
α (°)	90	90	90	90	73.373(2)	90	90	90
β (°)	90	90	93.0540(10)	99.905(2)	79.170(2)	95.4610(10)	96.941(2)	90
γ (°)	120	90	90	90	68.124(2)	90	90	90
V (Å^3)	6650.5(16)	2700.0(9)	3134.0(3)	4261.6(7)	1864.3(3)	3244.0(4)	3808.9(6)	2193.9(2)
Z	6	4	4	8	2	4	4	4
R1[a] (all data)	0.0471	0.0315	0.0301	0.0437	0.0658	0.0444	0.0407	0.0295
wR2[b] (all data)	0.1080	0.0678	0.0507	0.0681	0.1189	0.0805	0.0749	0.0501
R1 [($I > 2\sigma$)]	0.0406	0.0293	0.0234	0.0341	0.0408	0.0319	0.0344	0.0224
wR2 [($I > 2\sigma$)]	0.1026	0.0671	0.0481	0.0650	0.1042	0.0748	0.0730	0.0474
GOF[c]	1.079	1.052	1.032	1.122	1.021	1.048	1.173	1.050

[a] $R1 = \Sigma||F_o| - |F_c||/\Sigma|F_o|$. [b] $wR2 = (\Sigma(w(F_o^2 - F_c^2)^2)/\Sigma(w(F_o^2)^2))^{1/2}$. [c] $GOF = (\Sigma\, w(F_o^2 - F_c^2)^2/(n - p))^{1/2}$ where n is the number of data and p is the number of parameters refined.

temperature $^{31}P\{^1H\}$ and ^1H NMR spectroscopic analyses unambiguously demonstrate that oxidation of $Au_2^{I,I}$ chloride complexes **1** and **2** with 1 equiv of $PhICl_2$ and oxidation of $Au_2^{I,I}$ bromide complexes **5** and **6** with 1 equiv of Br_2 exclusively produces mixed-valent $Au_2^{I,III}$ compounds in solution. Two distinct peaks are apparent in the 121.5 MHz $^{31}P\{^1H\}$ NMR spectra of the $Au_2^{I,III}$ oxidation products **9**, **11, 15**, and **17**. For dppm complexes **9** (X = Cl) and **15** (X = Br), P−P coupling of 17 and 21 Hz is observed, respectively, whereas dcpm-bridged **11** (X = Cl) shows a much smaller coupling constant of 9 Hz. The coupling in **17** is too weak to be observed and two singlets are present in the $^{31}P\{^1H\}$ NMR spectrum. In the ^1H NMR spectra, the CH_2 resonance for the mixed-valent species **9**, **11**, **15**, and **17** appears as a doublet of doublets, due to coupling to two nonequivalent phosphorus nuclei. In contrast, this same resonance in the valence-symmetric bimetallic compounds **1**, **2**, **5**, **6**, **10**, **12**, **16**, and **18** shows a triplet splitting pattern. **9** was previously used as a starting material to prepare Au^{II}−aryl complexes and was reported to exist as a valence-symmetric, metal−metal bonded $Au_2^{II,II}$ dimer,[43] though no details of the synthesis or characterization were given. However, all of our spectroscopic and structural evidence clearly identifies **9** as a mixed-valent compound.

X-ray crystal structures for **2**, **9**, **10**, **14**, **16**, **17**, **18**, and **20** are depicted in Figure 1. Attempts to grow crystals of **6**, **11**, and **12** gave unsuitable material for X-ray diffraction. In all cases, typical Au−P and Au−X bond distances are observed; cif files for all structures are available in the Supporting Information. The crystal structure of **2** shows approximately linear coordination about the two Au^I atoms, with an average P−Au−Cl bond angle of 173.62(11)° for the two crystallographically independent molecules. An aurophilic interaction[44] is also apparent, with an average Au···Au separation of 3.262(9) Å. All Au^{III} centers possess a nearly square planar coordination geometry, as expected for a d^8 metal, whereas the Au^I atoms in mixed-valent **9** and **17** show the expected linear two-coordinate environment for d^{10} Au^I. The singly bridged framework with a methylene-spaced diphosphine ligand affords a very flexible geometry as is evident from the multitude of solid-state conformations shown in Figure 1, together with previously reported structures of **1**,[35,45] **5**,[39] and **15**.[39] Intramolecular π-stacking interactions contribute to the observed conformation of **16**; an obvious intra- or intermolecular ligand- or metal-based interaction is not apparent in X-ray crystal structures for any other complex. The solution NMR spectra of all $Au_2^{III,III}$ complexes are consistent with an average C_2 symmetry, indicating that the solid-state structures do not persist in solution.

Thermal Reduction Reactions. The Au^{III} bromide complexes are cleanly reduced to their respective Au^I precursors in the presence of an alkene, in complete exclusion of light. Dimeric compounds **16** and **18** and monomeric **19** and **20** react with *cis*-2-hexene, *trans*-2-hexene, 3,3-dimethyl-1-butene, 3-methyl-1-pentene, and *trans*-4-methyl-2-pentene to furnish the dibromoalkane product; where possible, only the diastereomer resulting from anti addition across the carbon−carbon double bond is observed. Figure 2 shows the time-dependent $^{31}P\{^1H\}$ NMR spectra for the thermal decay of **16** (R = Ph) and **18** (R = Cy) in 1.2 M 1-hexene/CH_2Cl_2; the spectra indicate that the thermal decay reaction proceeds as follows

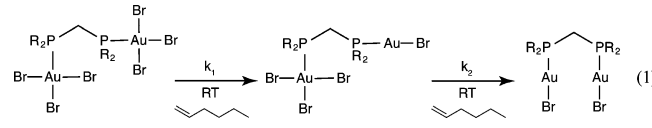

(1)

A minor and undetermined side product, estimated to be <5% in quantity, grows in at later time points of the decay of **16**. The very small amount of $Au_2^{I,III}$ present in the $t = 0$ spectrum of **18** appeared during the lag time between mixing the sample and acquisition of the first spectrum. Under the same conditions, solutions of the Au^{III} chloride complexes **9**−**14** do not smoothly undergo two-electron reductive elimination. Although the two-electron reduced species are observed in the ^{31}P NMR spectra, several intractable side products also appear, and we observe visual evidence for the formation of Au^0 in some cases. As the thermal reduction of the $Au_2^{III,III}$ bromide complexes proceeds and appreciable

(43) Usón, R.; Laguna, A.; Fernádez, E. J.; Mendia, A.; Jones, P. G. *J. Organomet. Chem.* **1988**, *350*, 129–138.
(44) Schmidbaur, H.; Schier, A. *Chem. Soc. Rev.* **2008**, *37*, 1931–1951.
(45) Healy, P. C. *Acta Crystallogr.* **2003**, *E59*, m1112−m1114.

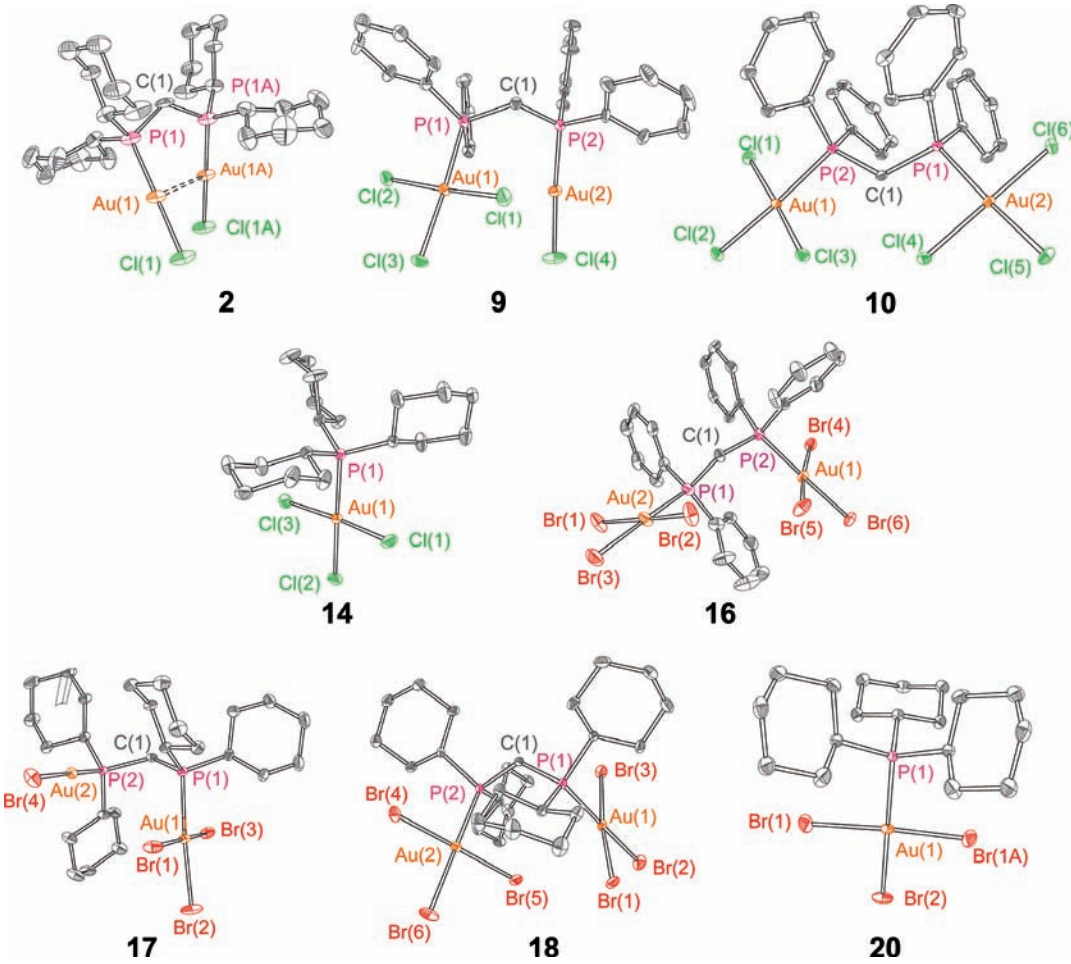

Figure 1. Crystal structures of **2**, **9**, **10**, **14**, **16**, **17**, **18**, and **20**. Ellipsoids are drawn at 50% probability level; hydrogen atoms and solvent molecules are omitted for clarity. All data were collected at 100 ± 2 K.

$Au_2^{I,I}$ complex is accrued, a competing comproportionation reaction between $Au_2^{III,III}$ reactant and $Au_2^{I,I}$ product is established as the concentration of the $Au_2^{I,I}$ increases

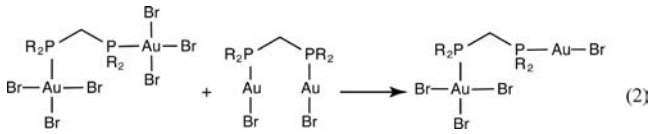

Equimolar mixtures of dppm-bound **16** and **5** react quite rapidly; within 90 min, quantitative formation of **15** is observed for a starting reactant concentration of ∼3 mM. The reaction between dcpm complexes **18** and **6** is much slower, but within 19 h a solution containing 6 mM each of **6** and **18** shows near complete formation of **17**. The transfer of halides between Au^{I} and Au^{III} centers is not unprecedented, and has been implicated as one of several steps involved in the halide redistribution that occurs when phosphine−gold(I) chloride complexes are oxidized with Br_2.[42]

The rate constants k_1 and k_2 (eq 1) listed in Table 2 were determined for the reactions of **16** and **18** with 1-hexene under pseudo-first-order conditions ([hexene] = 1.2 M, [Au] = 3−6 mM). The kinetics were ascertained by monitoring the disappearance of the single $^{31}P\{^1H\}$ NMR resonance of $Au_2^{III,III}$ complexes (for k_1) and the two $^{31}P\{^1H\}$ NMR resonances of the $Au_2^{I,III}$ complexes (for k_2). The pseudofirst order rate constant was determined from plots of $\ln([A]/[A]_o)$ vs time; $\ln([A]/[A]_o)$ was obtained from the relative integration of the $^{31}P\{^1H\}$ NMR signals of **16** and **18** and the sum of the integrations for the two signals of **15** and **17**. Linear plots were obtained, from which the values for the rate constants were extracted. In the case of **16**, k_1 was determined by only considering early time points, for which the concentration of **5** was low (<0.05[**16**]), and the comproportionation step shown in eq 2 could be ignored. For complex **18**, comproportionation with **6** occurs at an appreciably small rate such that deviations from linearity in the $\ln([A]/[A]_o)$ vs time plot are not observed over all time points. The rate constant for comproportionation was not determined for either bimetallic system owing to large associated errors with absolute concentration measurements from $^{31}P\{^1H\}$ NMR spectra.

The monomeric Au^{III} complexes likewise convert to the Au^{I} congeners in the presence of olefin. The reduction of **20** to **8** is very sluggish, requiring about a month to complete in 1 M olefin, and for this reason detailed kinetic studies of **20** were not pursued. After 12 h, only ∼10% of **19** converts to **7** in 1.2 M 1-hexene; in comparison a solution of dimeric **16** completely converts to fully reduced **5** in the same time frame. Stacked $^{31}P\{^1H\}$ NMR spectra for the reduction of **19** are shown in Figure S1 in the Supporting Information. The slope of a plot of $\ln([A]/[A]_o)$ vs time gradually increases in magnitude as the reduction of **19** proceeds to completion, indicating that the product **7** accelerates the reaction and a description of this system with pseudo-first-order kinetics is not valid. In a separate experiment, reduction of **19** in the presence of 2 equiv of **7**,

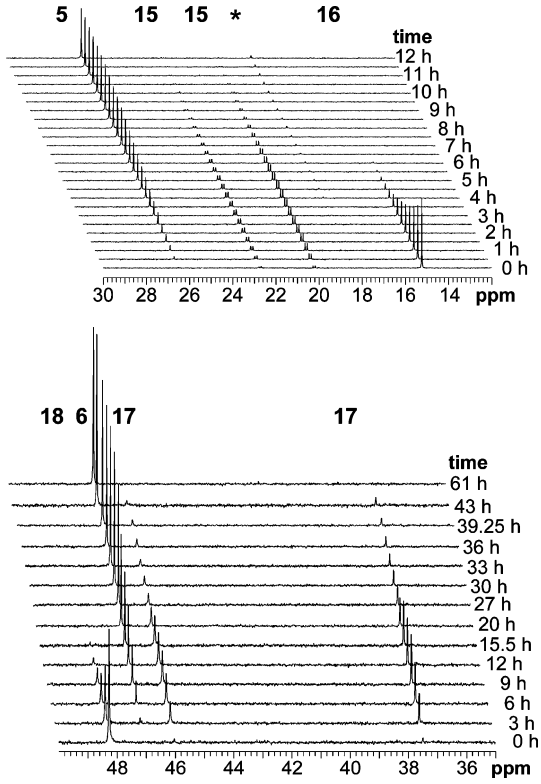

Figure 2. Time-dependent $^{31}P\{^1H\}$ NMR spectra for the thermal reduction of **16** (top) and **18** (bottom), at 293 ± 1 K in CH_2Cl_2 in the presence of 1.2 M 1-hexene. All spectra were recorded at 202.5 MHz and referenced to an external standard of 85% D_3PO_4. Compound numbers are diagonally aligned with their respective resonances, in addition to a minor impurity (*).

Table 2. Rate Constants for the Thermal Reduction of **16** and **18**[a]

	k_1 (min^{-1})	k_2 (min^{-1})
16	$(6.5 \pm 0.6) \times 10^{-3}$	$(6.1 \pm 0.5) \times 10^{-3}$
18	$(3.7 \pm 0.1) \times 10^{-3}$	$(1.66 \pm 0.03) \times 10^{-3}$

[a] Recorded in 1.2 M 1-hexene in CH_2Cl_2 at 20 ± 1 °C. Values are an average of two or more trials with standard errors.

under otherwise identical conditions, resulted in much more rapid consumption of **19**; ~60% conversion to **7** was observed in the first 12 h. The reduction of **19** (with no **7** initially) approximates pseudo-first-order behavior at early time points (t < 24 h), when the concentration of **7** is comparatively low. The apparent rate constant during this early time period is ~2 × 10^{-4} min^{-1}, an order of magnitude smaller than the rate constants for the bimetallic systems listed in Table 2.

Solution Photochemistry. The UV−vis absorption spectra (λ > 300 nm) of the gold halide compounds reported here are largely determined by X → Au^{III} charge transfer as shown by a comparison of the spectra of (i) chloride and bromide congeners and (ii) Au^{III} and Au^{I} analogues. Figure 3 displays the electronic spectral for the halide complexes of $Au_2^{III,III}$ cores, which are representative of a complex containing at least one Au^{III} center; spectra for all 20 complexes reported in this study can be found in Figures S2−S9. The Au^{III} complexes exhibit a distinct and intense low-energy absorption band that tails into the visible spectral region and is responsible for the red (X = Br) and yellow (X = Cl) colors observed for concentrated solutions of the complexes. As seen in Figure 3, the position of the low-energy absorption band is influenced primarily by the nature of the halide. Monomers and dimers with the same halide and similar phosphine substitution essentially absorb at the same

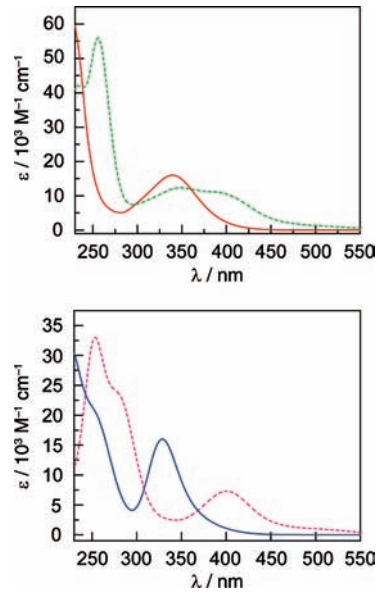

Figure 3. Overlaid electronic absorption spectra, measured in CH_2Cl_2 at room temperature. The spectra of **10** (—, red) and **16** (− − −, green) are shown on top, **12** (—, blue) and **18** (− − −, red) on the bottom set of axes.

energy for this low-energy maximum, though the extinction coefficient is augmented in the $Au_2^{III,III}$ dimers relative to their analogous $Au_2^{I,III}$ and Au^{III} complexes. As an example, the lowest-energy absorption maximum for **19** appears at 346 nm, shifting only minimally to the 349 nm low energy maximum of **16**. The bromide complexes possess overlapping low-energy absorption bands, which are most apparent in the spectra of $Au_2^{I,III}$ and $Au_2^{III,III}$ dppm complexes **15** and **16**, respectively. In other bromide complexes, a second band can be seen as a weak shoulder whereas the chloride complexes appear to show a single, generally sharper absorption band. The most distinguishing feature between the chloride and bromide series is the pronounced bathochromic shift of the low energy band of the latter series. The magnitude of this energy difference for the lowest energy transition is between 4000 and 5000 cm^{-1}, which is in accordance with the bathochromic shift of a halide based LMCT transition between halide and Au^{III}.[46] Of course, in the case of a d^{10} metal center, the LMCT transition is obviated. Au^{I} monomeric and dimeric halide complexes **1**−**8** are colorless, exhibiting absorption from the solvent cutoff wavelength to ≤270 nm.

When solution samples of Au^{III} complexes **9**−**20** are irradiated within their low-energy absorption manifold in the presence of alkene, clean conversion to the corresponding reduced species is observed. Unlike the thermal reaction chemistry, the photochemical reduction proceeds for both chloride and bromide metal complexes. Because the spectra of $Au_2^{III,III}$ and $Au_2^{I,III}$ complexes exhibit energetically similar maxima and lack an isosbestic point in the visible spectral region, $^{31}P\{^1H\}$ NMR was a more informative method for monitoring photochemical reactions. The $^{31}P\{^1H\}$ NMR spectral changes that accompany the irradiation of **12** and 1 M 1-hexene in CH_2Cl_2 shown in Figure 4 are representative of the irradiation of all $Au_2^{III,III}$ complexes with light coincident with their lowest-energy absorption band. When the photolysis of **12** is halted at an arbitrary and intermediate

(46) Lever, A. B. P. *Inorganic Electronic Spectroscopy*; Elsevier: New York, 1984; Chapter 5.

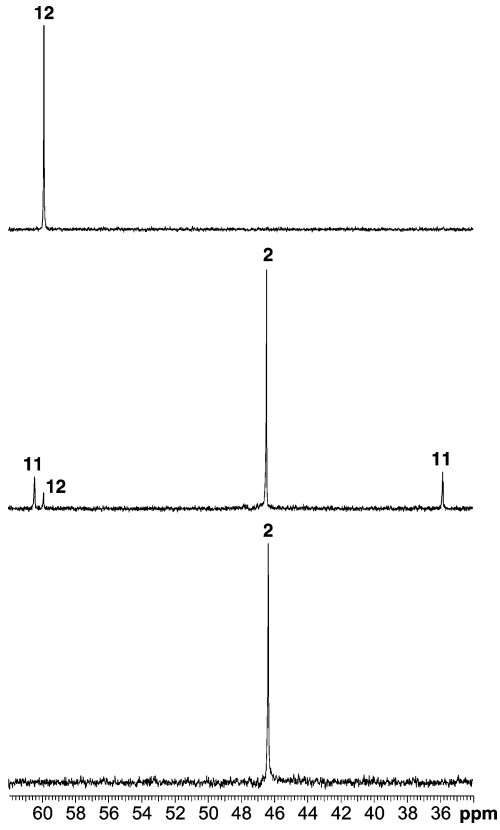

Figure 4. $^{31}P\{^1H\}$ NMR spectra of (top) the initial solution of **12** in 1 M 1-hexene, and under photolysis using light with $\lambda > 300$ nm at ~10 °C (middle) at an arbitrary midpoint during the photolytic reaction and (bottom) at the conclusion of the photolysis. Resonances for **2**, **11**, and **12** are indicated.

time point, all three $Au_2^{III,III}$, $Au_2^{I,III}$, and $Au_2^{I,I}$ complexes are present. Continued photolysis of the solution results in complete conversion to **2**. The overall photochemical transformation is

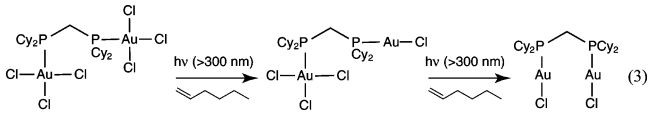

(3)

Photolysis of Au^{III} parent monomers proceeds directly to their Au^I relatives without the detection of an intermediate. For mono- and bimetallic gold−chloride complexes **9**−**14**, minor side products were frequently observed in the $^{31}P\{^1H\}$ NMR spectra immediately after photolysis. In all cases we estimate these impurities to comprise <10% of the product. We suspect that the phosphine is labilized and subsequently oxidized by the liberated Cl_2 or $Cl^{\bullet}$, though attempts to positively identify the minor side products were unsuccessful.

The dihaloalkane is obtained as the predominant trap product for photochemical reduction using a variety of mono-olefins. As with the thermal reduction experiments, a variety of asymmetrically substituted olefins was employed, allowing us to gain insight into the photochemical transformation. The product of direct, anti addition of X_2 across the double bond is obtained as the major organic product in all cases. However, unlike the thermal reaction chemistry, the syn-addition diastereomer is observed as a minor product for internal alkenes. Bromide complexes **15**−**20** all lead to the formation of ~30% syn-addition product as judged by integration of ^1H NMR spectra, whereas for chloride complexes, cyclohexyl-substituted

Table 3. Quantum Yields (Φ) for Photochemical Reduction of **9**−**20**[a]

compd	0.125 M	0.25 M	0.5 M	1 M
9	0.09(1)	0.089(1)	0.09(1)	0.14(2)
10	0.13(2)	0.16(3)	0.21(3)	0.14(4)
11	0.15(1)	0.16(1)	0.14(2)	0.17(3)
12	0.23(3)	0.24(2)	0.25(2)	0.26(4)
13	0.11(1)	0.12(1)	0.13(1)	0.13(1)
14	0.14(3)	0.15(2)	0.16(3)	0.16(1)
15	0.024(3)	0.018(1)	0.020(2)	0.018(4)
16	0.10(3)	0.12(5)	0.15(3)	0.14(2)
17	0.08(2)	0.10(1)	0.11(1)	0.11(2)
18	0.18(1)	0.17(2)	0.20(3)	0.20(2)
19	0.15(1)	0.15(1)	0.17(2)	0.20(3)
20	0.16(3)	0.15(1)	0.14(1)	0.15(2)

[a] Measured in CH_2Cl_2 with 1-hexene trap in the stated concentrations. All values are the average of three independent trials.

complexes **12** and **14** give a smaller percentage of the syn product, generally 10−20%, as compared to ~30% for phenyl-substituted **10** and **13**. The amount of syn-addition product is independent of the alkene's stereochemistry; cis and trans alkene isomers result in nearly identical ratios of the syn and anti-addition diastereomers for a given complex. The ^1H NMR spectra of photochemical reaction solutions reveal that the gold complexes described here catalytically isomerize alkenes when irradiated hence leading to mixtures of dibromoalkane diastereomers. A 0.5 M cis-2-hexene solution in the presence of 33 mM **19** is stable in the dark; but as shown in of Figure S17, photolysis of the solution at $\lambda > 300$ nm for about 5 min showed 60% conversion to trans-2-hexene with concomitant formation of **7**. This chemistry is quite general and is replicated using different Au^{III} complexes and alkenes. The Au^I complexes also effect alkene isomerization, and prolonged photolysis of a cis alkene in the presence of **1**−**8** proceeds to give the thermodynamic cis/trans ratio of the alkene.

Quantum yields listed in Table 3 for the reduction of mono- and bimetallic Au^{III} halide compounds **9**−**20** in varying concentrations of 1-hexene were measured using potassium ferrioxalate actinometry. Chloride complexes **9**−**14** were excited with monochromatic 320 nm light, whereas bromide complexes **15**−**20** were excited at 370 nm. For a given compound, the quantum yield is similar within experimental error for all trap concentrations. $Au_2^{III,III}$ dimers consistently exhibit higher quantum yields than their $Au_2^{I,III}$ congeners. This effect is most dramatic for **15,** for which $\Phi \approx 2\%$, compared to the fully oxidized **16**, which has quantum yields ranging from 10% to 15% over the range of trap concentrations. The data in Table 3 also show that, in most case, complexes with cyclohexyl-substituted phosphines demonstrate higher solution quantum yields than their phenyl-substituted analogues. The lone exception to this trend is complex **19**, which has a minimally higher quantum yield than **20**. Finally, in comparing chloride complexes to their bromide analogues, the chloride complexes generally have slightly higher quantum yields.

Solid-State Photochemistry. Irradiation of solids of Au^{III} dimeric bromide complexes **16** and **18** and monomeric bromide complexes **19** and **20** with light enveloping the low-energy absorption band gives the corresponding reduced species as major products. Solid-state photolysis experiments were conducted in an evacuated H-shaped cell. The gold complex was housed in one compartment, and the other compartment was frozen in liquid N_2 to trap and isolate volatile photoproducts. Upon completion of the photolysis, the solid was taken up in CH_2Cl_2 and analyzed by $^{31}P\{^1H\}$ NMR. Figure 5 shows the

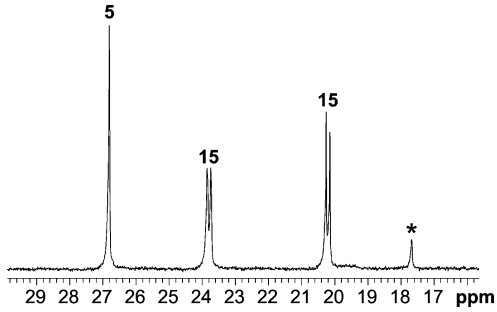

Figure 5. $^{31}P\{^1H\}$ NMR spectrum of the product following photolysis of a solid-state sample of **16** for 2 h, using light with $\lambda > 300$ nm at 10 °C for 2.5 h. Resonances for **15** and **5** are observed, in addition to an unidentified side product (*). Spectrum was recorded in CH_2Cl_2 at 202.5 MHz and is referenced to an external standard of 85% D_3PO_4.

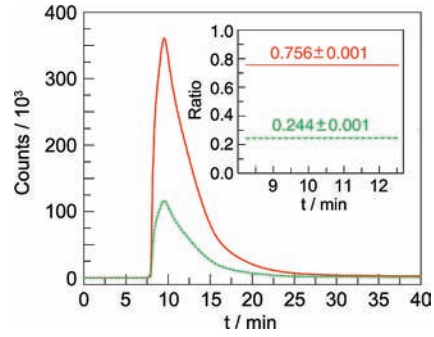

Figure 6. Real-time mass spectrometry trace for liberated Cl_2 following photolysis of a solid sample of **12**. Depicted are total ion counts for ^{35}Cl (—, red) and ^{37}Cl (— — —, green), which form upon fragmenting Cl_2 in the ionization chamber. The inset shows the ratios of the two isotopes during the time range when the ion counts are greater than 1/2 × max.

$^{31}P\{^1H\}$ NMR spectrum that results when a thin layer of solid **16** was photolyzed at 10 °C for 2.5 h. The spectrum shows a mixture of **15** and **5** in yields of ~60% and 30% relative to starting **16,** with a minor side product also evident. No detectable amount of **16** is observed in the $^{31}P\{^1H\}$ NMR. This observation is consistent with either the complete photochemical conversion of the reactant or the comproportionation of **16** with **5** upon taking up the solid photoproducts in CH_2Cl_2 for NMR analysis. The $^{31}P\{^1H\}$ NMR spectra for all other solid state photolysis experiments are collected in Figures S10−S16. A volatile photoproduct was isolated from vacuum transfer within the H-shaped cell onto frozen H_2O. Upon thawing, treatment with *N*,*N*-diethyl-1,4-phenylenediamine sulfate (DPD) identified the photoproduct as bromine, which oxidizes colorless DPD to produce the intensely pink $[DPD]^{\bullet+}$ (see Figure S18).[47,48]

Solid-state irradiation of chloride complexes also results in photoreduction. Photolyses of **12** and **14** form **2** and **4**, respectively, as the major species. For these reactions, many of the minor side products exhibit ^{31}P NMR shifts very similar to **2** and **4**, possibly indicating chlorination of C−H bonds on the phosphine. Compounds **10** and **13**, with phenyl-substituted phosphines, produce **1** and **3**, respectively, in lower yields. Several decomposition products are evident in the NMR spectra, and we suspect phosphine oxidation of the aryl-substituted phosphine by liberated chlorine to be a major culprit. We attempted to isolate the chlorine the same way as with bromine, by trapping in frozen water, but in all cases the DPD test showed no evidence for successful isolation of Cl_2. The inability to isolate Cl_2 in this manner most likely is a result of the high reactivity and volatility of chlorine, which leads to a very low trapping efficiency in our setup. To demonstrate formation of Cl_2, the condensed gases following photolysis of **12** in the solid state were thawed and flowed into a mass spectrometer. Figure 6 shows the MS trace for ^{35}Cl and ^{37}Cl, which form upon fragmentation of Cl_2 in the ionization chamber. Upon thawing, a sharp increase in signal from baseline values is observed. Also, the isotopic ratio of 0.756 ± 0.001 for ^{35}Cl is consistent with the literature value of 0.758 for the natural abundance of ^{35}Cl.[49]

The reverse reaction in solid-state photolysis experiments, that is, the reaction of Au^I centers with elemental X_2 to reform Au^{III}, is spontaneous and rapid. When solid samples of dimeric **6** or monomeric **7** are exposed to excess Br_2, an immediate color change from white to dark orange is observed as the Br_2 vapors come into contact with the solid. After brief (<10 min) exposure, solution $^{31}P\{^1H\}$ and ^1H NMR spectra of the product shows clean conversion to the corresponding oxidized species **18** or **19**. Brief exposure of colorless **2** to Cl_2 gas leads to an immediate color change to yellow, and $^{31}P\{^1H\}$ NMR of the dissolved product shows a mixture of $Au_2^{I,III}$ (**11**) and $Au_2^{III,III}$ (**12**), in addition to starting material. Prolonged exposure to an excess of Cl_2 gas leads to an intractable mixture of decomposition products.

Discussion

The efficient reductive elimination of halogen may be thermally and photochemically driven from Au(III) centers of mono- and bimetallic centers. In solution, halogen must be chemically trapped. Solutions of mono- and bimetallic compounds **15**−**20**, in the presence of an olefin and in the absence of light, are cleanly reduced to their respective Au^I complexes at room temperature, over the course of hours to days.

Analysis of the regio- and stereochemistry of the dihaloalkane product of a variety of monoalkene traps provides insight into the mechanism of thermal reductive elimination. For alkenes with two prochiral centers (e.g., *cis*-2-hexene, *trans*-2-hexene, and *trans*-4-methyl-2-pentene), a single diastereomer is obtained that is consistent with an electrophilic mechanism proceeding through a bromonium intermediate to furnish the anti addition product.[50] These results contrast the products anticipated from a radical mechanism, which is expected to involve a planar sp^2 radical that can undergo both syn and anti addition to give a 50:50 mixture of both diastereomers, with possible rearrangement and oligomerization of radical intermediates. For 3-methyl-1-pentene and 3,3-dimethyl-1-butene, it is not possible to distinguish syn and anti addition products, but a radical intermediate would presumably rearrange to a stable tertiary radical, leading to products of altered connectivity. Such rearranged products are not observed. Comparison of the thermal elimination kinetics of $Au_2^{III,III}$ complexes with Au^{III} monomers is revealing. The rate constant for early time points in the reduction of monomer **19** is an order of magnitude lower than the rate constants for the bimetallic complexes **16** and **18**. These data suggest that the two gold atoms in the tethered dimers interact to facilitate the reductive elimination of halogen from

(47) Nickel, U.; Chen, Y.-H.; Schneider, S.; Silva, M. I.; Burrows, H. D.; Formosinho, S. J. *J. Phys. Chem.* **1994**, *98*, 2883–2888.
(48) Bader, H.; Sturzenegger, V.; Hoigné, J. *Water Res.* **1988**, *22*, 1109–1115.
(49) Lide, D. R., Ed. *CRC Handbook of Chemistry and Physics*, 84th ed.; CRC Press: Boca Raton, FL, 2003.
(50) Bruice, P. Y. *Organic Chemistry*, 4th ed.; Prentice Hall; Upper Saddle River, NJ, 2004.

both the $Au_2^{III,III}$ and $Au_2^{I,III}$ complexes. In line with this observation, the reduction of **19** is promoted by **7**, which results in deviations from pseudo first order behavior when the concentration of **7** is appreciable. Halide-bridged intermediates have been postulated in ligand redistribution reactions,[42] so it is possible that such an intermediate, albeit short-lived, could form when **19** is in the presence of **7**. As we have shown,[51,52] bridged intermediates are crucial to the facilitating reductive elimination from bimetallic cores.

Product analysis reveals that the photochemical reaction mechanism deviates from that of the thermal reaction. Excitation of the low-energy absorption bands of Au^{III} complexes yields significant amounts of the syn-addition haloalkane product, in addition to the major anti-addition diastereomer that is exclusively observed in the thermal reaction. The presence of the syn-addition diastereomer is partly accounted for by the observation deduced from Figure S17, which shows that phosphine-gold compounds photocatalyze the cis/trans isomerization of alkenes. Nonetheless, the observed ratio of syn to anti addition products is higher than the ratio of photoisomerized alkene, particularly for photoreactions involving trans alkenes. These results suggest that a radical-based mechanism is operative in addition to an electrophilic mechanism, which should exclusively lead to anti addition across the carbon−carbon double bond of the trap.

The photochemical reaction occurs upon excitation of absorption bands with significant ligand-to-metal charger transfer (LMCT) character. The significant shift of the low-energy absorption band upon substituting chlorides for bromides in otherwise identical complexes is a qualitative indicator of significant LMCT character.[53] LMCT excitation of late-metal halide complexes typically results in liberation of halogen radicals and a formal one-electron reduction of the metal.[54] This behavior has been extensively studied for the $[Pt^{IV}Cl_6]^{2-}$ anion, which photochemically reduces to the $[Pt^{II}Cl_4]^{2-}$ anion, in a process involving a $[Pt^{III}Cl_5]^{2-}$ intermediate.[55] Similar behavior is postulated for $Au^{III}Cl_4^-$ ion.[32] For either Pt or Au systems, extensive thermal chemistry follows the initial one-electron photoreduction. To this end, the Au^{III} photochemistry reported here is exceptional inasmuch both the inorganic and organic photoproducts are consistent with X_2 elimination. If $X^\bullet$ is liberated upon LMCT excitation, then (i) cage escape of $X^\bullet$ is minimal based on the haloalkane product analysis and (ii) the subsequent elimination of a second $X^\bullet$ must be sufficiently rapid to overwhelm recombination of $X^\bullet$ and the Au^{II} primary photoproduct since haloalkane products characteristic of radical-based chemistry are produced in minor quantities. Solid-state photolysis reactions provide further evidence for X_2 elimination. Au^I complexes and X_2 are produced under conditions where radical trapping or stabilization is not feasible. Thus a stepwise elimination $X^\bullet$ to furnish X_2 must be extremely rapid. Alternatively, $X^\bullet$ is not the predominant photoproduced species. Terminal ligands in the equatorial waist of the core of two-electron mixed-valence cores exhibit a propensity to migrate to and from bridging positions, owing to low reorganization energies arising from the ability of the bimetallic core to preserve the electronic and coordination asymmetry accompanying rearrangement.[51,52,56] Such a migration permits X_2 elimination and averts $X^\bullet$ formation. By spanning the $Au_2^{I,I}$ and fully oxidized $Au_2^{III,III}$ species, the two-electron mixed valence $Au_2^{I,III}$ complex sustains the multielectron reactivity of the bimetallic systems of Chart 1. The photochemistry of cycles involving two-electron metal complexes was previously confined to those compounds containing a metal−metal bond. In these cases, the metal−metal bond provides a visible chromophore from which to drive the photoreductive elimination. As we show here, when no metal−metal bond exists, the LMCT transition of high oxidation state metals may be exploited as a visible chromophore and a productive two-electron chemistry may be achieved.

Finally, the observation that X_2 thermally adds to the Au^I compounds in the solid state to give the Au^{III} photoreactants is noteworthy. Under the same physical conditions, the reaction may be reversed using light, establishing that the photoreaction is energy storing. The ability to effect trap-free halogen photoelimination greatly eases the complexity of the criteria for the design of a solar energy HX-storage cycle.

Acknowledgment. We thank Y. Surendranath for technical assistance in acquiring mass spectrometric data. This work was supported by NSF Grant No. CHE-0750239. Grants from the NSF also supported the MIT Department of Chemistry Instrumentation Facility (CHE-9808061, DBI-9729592). T.S.T. acknowledges the Fannie and John Hertz Foundation for a predoctoral fellowship.

Supporting Information Available: NMR spectra for the thermal reduction of **19**, electronic absorption spectra for all gold complexes, $^{31}P\{^1H\}$ NMR spectra for solid-state photolysis products, absorption spectrum of the chemical assay for Br_2, ^1H NMR spectrum showing organic photoproducts of photolysis of *cis*-2-hexene with **19**, ^1H and $^{31}P\{^1H\}$ NMR spectra for **11**, and crystallographic information files (CIFs). This material is available free of charge via the Internet at http://pubs.acs.org.

JA9009937

(51) Gray, T. G.; Veige, A. S.; Nocera, D. G. *J. Am. Chem. Soc.* **2004**, *126*, 9760–9768.
(52) Esswein, A. J.; Veige, A. S.; Nocera, D. G. *Organometallics* **2008**, *27*, 1073–1083.
(53) Lever, A. B. P. Charge Transfer Spectra. *Inorganic Electronic Spectroscopy*, 2nd ed.; Elsevier: New York, 1984; pp 203−375.
(54) *Photochemistry of Coordination Compounds*; Balzani, V., Carassiti, V. ; Academic Press: London, 1970.
(55) Goursot, A.; Kirk, A. D.; Waltz, W. L.; Porter, G. B.; Sharma, D. K. *Inorg. Chem.* **1987**, *26*, 14–18.
(56) Veige, A. S.; Gray, T. G.; Nocera, D. G. *Inorg. Chem.* **2005**, *44*, 17–26.